Electronic Supplementary Information

On-demand engineering of metal-doped porous carbon nanofibers as efficient bifunctional oxygen catalysts for high-performance flexible Zn-air batteries

Khang Ngoc Dinh,[a,b,c] Zengxia Pei,[c] Ziwen Yuan,[c] Van Chinh Hoang,[c] Li Wei,[c] Qianwei Huang,[d] Xiaozhou Liao,[d] Chuntai Liu,[e] Yuan Chen,[c*] Qingyu Yan[a,b*]*

a. Energy Research Institute @ NTU (ERI@N), Interdisciplinary Graduate School, Nanyang Technological University, Singapore 637553, Singapore. Email: alexyan@ntu.edu.sg

b. School of Materials Science and Engineering, Nanyang Technological University, Singapore 639798, Singapore.

c. School of Chemical and Biomolecular Engineering, The University of Sydney, Sydney, NSW 2006, Australia Email: yuan.chen@sydney.edu.au (Y. Chen), zengxia.pei@sydney.edu.au (Z. Pei)

d. School of Aerospace Mechanical and Mechatronic Engineering, The University of Sydney, Sydney, NSW 2006, Australia.

e. Key Laboratory of Materials Processing and Mold, Ministry of Education, Zhengzhou University, Zhengzhou 450002, China.

Materials.

Nafion perfluorinated resin solution (5%), 20 wt.% Pt/C, iron(III) nitrate nonahydrate ($Fe(NO_3)_3.9H_2O$, ≥99.95%), Cobalt(II) nitrate hexahydrate ($Co(NO_3)_2.6H_2O$, ≥98%), glycerol (≥99.5%), polyacrylonitrile (PAN, average Mw 150,000), isopropyl alcohol (IPA, 99%), N,N-dimethylformamide (DMF, 99.8%), hydrochloric acid (HCl, 37%), potassium hydroxide (KOH, 99.99%), were purchased from Sigma-Aldrich (Australia). Perchloric acid ($HClO_4$, 70%) was purchased from Ajax Chemicals. Iridium oxide (IrO_2, 99.9%) was purchased from Fuel Cell Store (US). All chemicals and materials were used without further purification.

Synthesis of CoFe-glycerate microspheres

Monodisperse CoFe-glycerate microspheres were prepared by a solvothermal method. In a typical synthesis, 0.1875 mmol $Co(NO_3)_2 \cdot 6H_2O$, 0.1875 mmol $Fe(NO_3)3 \cdot 9H_2O$ and 5 mL of glycerol were dissolved into 40 mL of isopropanol, and the solution was stirred until a clear orange solution is formed. Then, the above mixture solution was then transferred to a 100-mL stainless-steel Teflon-lined autoclave and heated in an electric oven at 180 ^oC for 6 hours. After cooling down to room temperature, the precipitate was collected by centrifugation and subsequently rinsed with technical grade ethanol for at least 5 times, followed by drying in a vacuum oven at 60 ^oC overnight.

Preparation of DMPCFs and PAN carbon nanofibers

600 mg of polyacrylonitrile (PAN) was dissolved in 6 g of N,N-dimethylformamide (DMF) by vigorous stirring overnight. 300 mg of CoFe-glycerate microspheres were added and dispersed under sonication for 5 hours. The solution was then further stirred for 10 hours to obtain the electrospinning precursor. The precursor was filled into a plastic syringe with a #21

needle and electrospun with a flow rate of 0.9 ml h^{-1}, an applied voltage of 20 kV, and a distance between the nozzle tip and the collector of 15 cm. Copper foil was wrapped on a drum rotating at 300 rpm, which is used as a collector. Afterward, the as-spun fibers were heated from room temperature to 280 ℃ for 2 h at the heating rate of 5 ℃ min^{-1} in air. Then, the as-stabilized fibers were pyrolyzed at 900 ℃ for 3 h at a ramping rate of 2 ℃ min^{-1} under Ar: H_2 (95:5, v/v) atmosphere. The obtained sample was etched by 4 M HCl for 24 h to remove the CoFe-template, followed by rinsing with deionized water repeatedly to wash off the metal chlorides residue. Finally, the MDPCFs were obtained after drying in a vacuum oven at 60 ℃ overnight.

MDPCFs were also fabricated using precursors containing different CoFe-glycerate microspheres to PAN mass ratios (1:1, 1:3, 1:4) by adjusting the mass of CoFe-glycerate to 600 mg, 200 mg, and 150 mg, respectively.

PAN carbon nanofibers were prepared under the same electrospinning conditions and pyrolyzed in the same conditions as that of the MDPCFs without the addition of CoFe-glycerate microspheres.

Fabrication of the polyacrylate hydrogel solid-state electrolyte

In a typical synthesis, 5 mL of concentrated sodium hydroxide solution (NaOH, 20 M) was added dropwisely into an aqueous solution of acrylic acid monomer (7.2 mL, 99.5 wt%) under vigorous stirring. While being stirred, MBAA as cross-linker was added, followed by the introduction of 120 mg of ammonium persulfate ($(NH_4)_2S_2O_8$) as the initiator. The solution was then stirred for another hour at room temperature (25 °C), followed by degassing to remove any dissolved oxygen. After sealing under N_2, the polymerization was accelerated at

60 °C for 2 h. Finally, the as-prepared polymer was peeled off and dried in an electric oven at 80 °C overnight.

Before usage, the dry gel was soaked in 500 mL solution of 6 M KOH with/without 0.2 M $Zn(CH_3COO)_2$ for 24 hours to achieve the equilibrium state. The as-obtained hydrogel could then be readily used as the solid-state electrolyte for ZABs.

Structure and surface characterization.

The crystallinity of synthesized carbon nanofiber materials was examined using X'Pert PANalytical X-ray diffractometer equipped with Cu Kα radiation (λ = 1.5406 Å) at an acceleration voltage and an emission current of 45 kV and 40 mA, respectively. XRD patterns were obtained at a scanning rate of 0.06° s^{-1}, with a step size of 0.01°.

The morphology and structure of the materials were characterized by scanning electron microscopy (SEM, ULTRA Plus, Zeiss) and transmission electron microscopy (TEM, JEOL, Model JEM-2100F) operating at 200 keV. The high-resolution TEM (HRTEM), high-angle annular dark-field scanning transmission electron microscopy (HAADF-STEM) and energy-dispersive X-ray spectroscopy (EDS) elemental mapping were performed on FEI Themis‑Z Double-corrected microscope.

The X-ray photoelectron spectroscopy (XPS) was conducted on an ESCALAB 250 photoelectron spectroscopy (Thermo Fisher Scientific) under pressure of 1.2×10^{-9} mbar using monochromatic Al Kα X-ray beam (1486.6 eV) at 100 W at an incident angle of 45°. The X-ray spot size is 400 μm. The voltage step size was 1 eV for survey spectra and 0.1 eV for high-resolution scans. The dwell time at every step was 50 ms and pass energy was 50 eV. All binding energies were charge corrected to the adventitious C 1s peak at 284.8 eV. The

chemical states of each element were appointed based on the NIST XPS Standard Reference Database 20. The atomic composition was computed based on the area of fitted peaks.

Raman spectra were recorded on a Raman spectrometer (Renishaw InVia Qontor confocal spectrometer with an upright microscope) in the range of 100-2000 cm^{-1} at the laser excitation wavelength of 532 nm.

The water contact angle was measured using a Drop Shape Analyzer (Krűss, DSA 25) using 6 M KOH solution as the liquid of interest. The droplet volume was set to be 400 µl for consistency

The surface area, total pore volume, and pore size distribution of the sample were derived from N_2 (77.4 K) adsorption–desorption isotherms collected on Quanta Chrome, Autosorb-1. The surface area was elucidated using a Brunauer-Emmett-Teller (BET) method in the linear range of P/P_0 = 0.1-0.3. The total pore volume was measured using a single point absorption at P/P_0 of 0.99.

Electrochemical measurements.

Electrochemical measurements were performed using a standard three-electrode configuration connected to a rotating disk electrode (RDE, PINE Research Instrumentation) at a rotation speed of 1600 rpm on an electrochemical workstation (CHI 760D CH Instrument). Catalysts were deposited on rotating disk glassy carbon electrodes (RDE, 5mm in diameter) as working electrodes. Pt mesh (or graphite rods for OER) and Hg/HgO electrodes serve as the counter electrode and the reference electrode, respectively.

The recorded potential was converted to a reversible hydrogen electrode (RHE) according to the Nernst equation: $E_{vs.\ RHE} = E_{vs.\ Hg/HgO} + 0.059 \times pH + 0.098$. The loading mass was 200 µg

cm^{-2} for both the non-noble metal catalysts and the referenced noble-metal materials (20 wt.% Pt/C, Sigma-Aldrich, and IrO_2, Fuel Cell Store).

Before the ORR/OER measurements, the electrolyte (0.1 M KOH or 0.1 M $HClO_4$) was purged by O_2 or Ar flow till saturation. CVs were performed in O_2- and Ar-saturated electrolyte with a scan rate of 20 mV s^{-1}. Linear sweep voltammograms for ORR/OER were acquired at a scan rate of 5 mV s^{-1} in the potential range of 0.2–2 V vs. RHE.

The half-cell reaction stability was evaluated by chronoamperometry tests at a constant potential (0.65 V vs. RHE for ORR and 1.6 V vs. RHE for OER). The long-term durability of the catalysts was assessed by continuous CVs at a scan rate of 50 mV s^{-1} (from 0.9-0.6 V for ORR and 1.3-1.6 V for OER). The electrochemical impedance spectroscopy (EIS) measurements were performed at a frequency range of 100 Hz to 1 MHz at an amplitude of 10 mV. All results were corrected for all ohmic (IR) losses throughout the system based on the solution resistance obtained from the EIS.

The Faradaic efficiency was done in an O_2-purged close H-shape cell (counter electrode was put in the different chamber). The headspace of the chamber containing the working electrode is 20.0 mL. A constant current of 10 mA was applied for 60 minutes. The gas generated was determined by taking 500 µL of the gas sample in the chamber containing the working electrode to gas chromatography. The Faradaic efficiency was then calculated as the ratio of the measured amount of gas and the theoretical amount of gas (based on Faraday's law).

The electrochemical surface area (ESCA) was estimated from the double-layer capacitance (C_{dl}) of the films. The C_{dl} was determined by simple cyclic voltammetry (CV) method. The CV was conducted in a potential window (0.2-0.3 V *vs.* Hg/HgO) at which no faradaic processes occur at various scan rates of 20, 40, 60, 80, 100, and 120 mV s^{-1}. Then capacitive current (j_{anodic} - $j_{cathodic}$) at 0.25 V *vs.* Hg/HgO was plotted against various scan rates, while the slope obtained was divided by two to acquire the C_{dl}. The specific capacitance can be

converted into an electrochemical active surface area (ECSA) using the specific capacitance value for a flat standard with 1 cm^2 of real surface area. The specific capacitance for a flat surface is normally found to be 20-60 μF cm^{-2}.[S1, S2] In our calculations of ECSAs, we took the average value of 40 μF cm^{-2}.

Calculated electrochemical active surface area:

$$A_{ECSA} = \frac{C_{dl}\ \mu F\ cm^{-2}}{40\ \mu F\ cm^{-2}\ per\ cm^2_{ECSA}}$$

Oxygen reduction reaction kinetics

The ORR kinetics were evaluated by using different rotational speed linear sweep voltammograms. The electron transfer number (n) in oxygen reduction was then determined according to the Koutecky–Levich (K–L) equation:

$$\frac{1}{j} = \frac{1}{j_k} + \frac{1}{j_L} = \frac{1}{j_k} + \frac{1}{B\omega^{1/2}}$$

$$B = 0.2nFC_0D_0^{2/3}v^{-1/6}$$

In which,

B: Levich slope,

j_K: kinetic current

j: measured total current

ω: electrode rotation rate (in revolutions per minute, rpm). As the rotation speeds are in rpm, the constant factor 0.2 is used.

n: number of electrons transferred for each oxygen molecule

F: Faraday constant (F= 96485 C mol^{-1})

D_{O2}: O_2 diffusion coefficient in 0.1 M KOH (D_{O2}= 1.9 x 10^{-5} cm^2 s^{-1})

v: kinetic viscosity (0.01 cm^2s^{-1})

C_{O2}: concentration of O_2 in O_2-saturated 0.1 M KOH solution (C_{O2}= 1.2 x 10^{-6} mol cm^{-3}).

The rotating ring-disk electrode (RRDE) tests were conducted with a Pt ring surrounding a 5.5 mm diameter glassy carbon electrode. Based on the following expressions, the electron transfer number (n) and hydrogen peroxide (H_2O_2) yield were calculated:

$$n = \frac{4i_d}{i_d + \frac{i_r}{N}}$$

$$\%HO_2^- = \frac{200i_r}{N(i_d + \frac{i_r}{N})}$$

In which,

i_r: the ring current

i_d: the disk current

N: current collection efficiency of the Pt ring. N was determined to be 0.38

Zinc-Air Battery Assembly and Performance Evaluation

Assembly of rechargeable aqueous Zn–Air batteries

Rechargeable Zn–air batteries were assembled using on a home-made electrochemical cell, in which a catalyst-loaded carbon cloth gas diffusion layer (with an effective area of 1.0 cm^2 and allows O_2 from ambient air to reach the catalyst sites) and a pre-polished Zn plate (0.5 mm in thickness) were used as an air cathode and an anode, respectively. For primary ZABs, 6 M

KOH was employed as the electrolyte, while 6 M KOH with 0.2 M $Zn(CH_3COO)_2$ was used as an electrolyte for rechargeable ZABs.

Regarding air cathode preparation, the catalysts slurry was firstly prepared by dispersing the catalysts in IPA/Nafion solution. Air cathodes were then constructed by uniformly drop-casting the catalyst slurry on the carbon cloth gas diffusion layer followed drying in a vacuum oven at 60 ^oC overnight. The reference catalyst mixture is made of commercial Pt/C and IrO_2 catalysts with a mass ratio of 1 to 1. The total mass loadings of the catalysts in each ZAB was 1.0 mg cm^{-2}.

Solid-state Zn-air batteries

The MDPCF catalyst was drop-casted onto a carbon cloth with a mass loading of 1.0 mg cm^{-2}. This catalyst-loaded carbon cloth was then employed as an air-cathode for the flexible ZAB; while, a pre-polished zinc foil (0.05 mm in thickness) was used as an anode.

The A-PAA hydrogel saturated with KOH or KOH+$Zn(CH_3COO)_2$ was adopted as the solid-state electrolyte. The flexible ZAB was then assembled with the air cathode and the Zn anode on the two sides of the hydrogel.

Battery performance testing

The galvanostatic discharging/charging voltage profiles were conducted on a LAND CT2001A multichannel battery testing system. Specific capacities were determined by galvanostatic discharge profiles normalized to the mass of Zn consumed. The round-trip efficiency was obtained from the ratio of discharge voltages to charge voltage. The power densities were computed by P = V x j. Cycling test for aqueous ZABs was performed at the current density of 10 mA cm^{-2} (10 minutes per cycle, discharge for 5 minutes, then charge for

5 minutes). Likewise, the solid-state ZABs were cycled at the current density of 2 mA cm^{-2} (10 minutes per cycle, discharge for 5 minutes, then charge for 5 minutes).

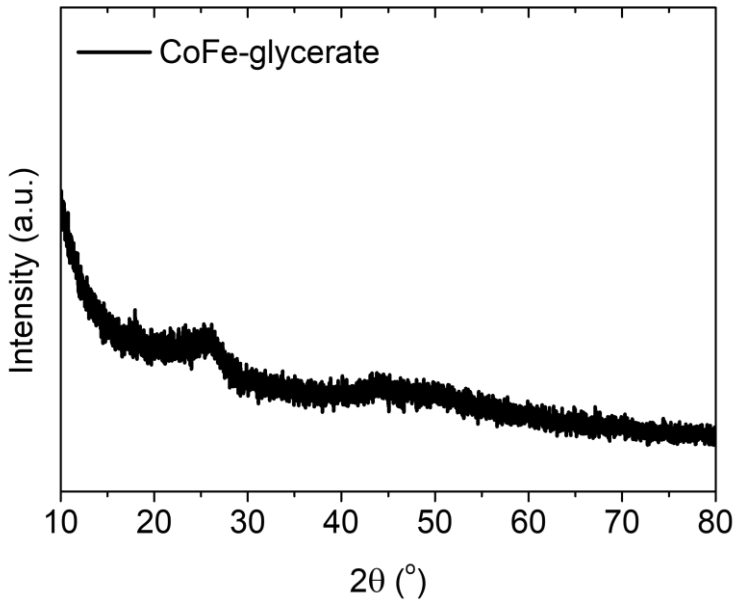

Figure S1. XRD pattern of CoFe-glycerate microspheres.

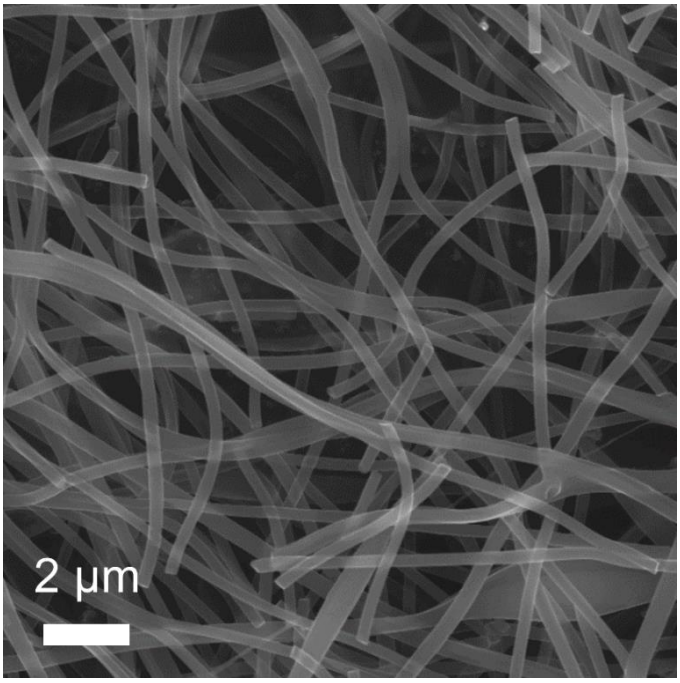

Figure S2. An SEM image of pristine PAN fibers.

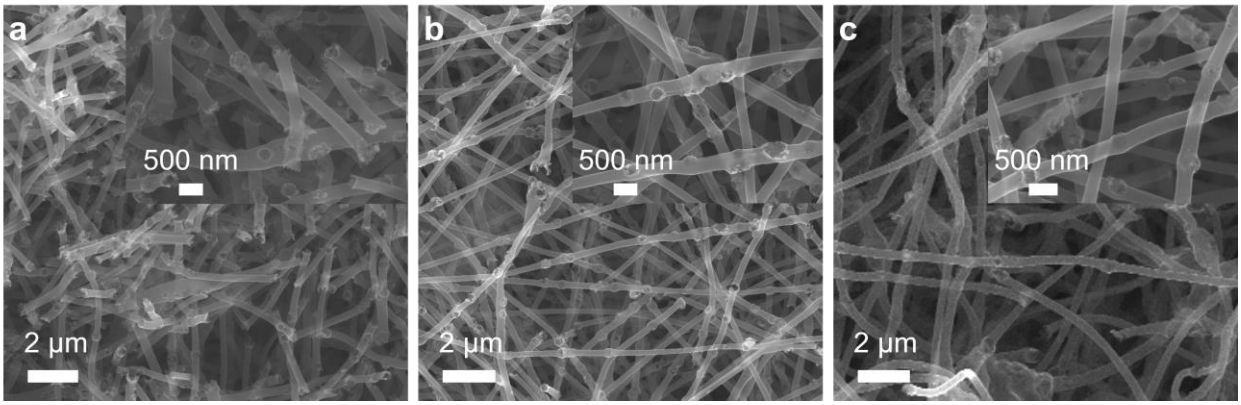

Figure S3. SEM images of MDPCFs synthesized at different CoFe-glycerate microspheres to PAN mass ratios (a) 1:1, (b) 1:3, and (c) 1:4.

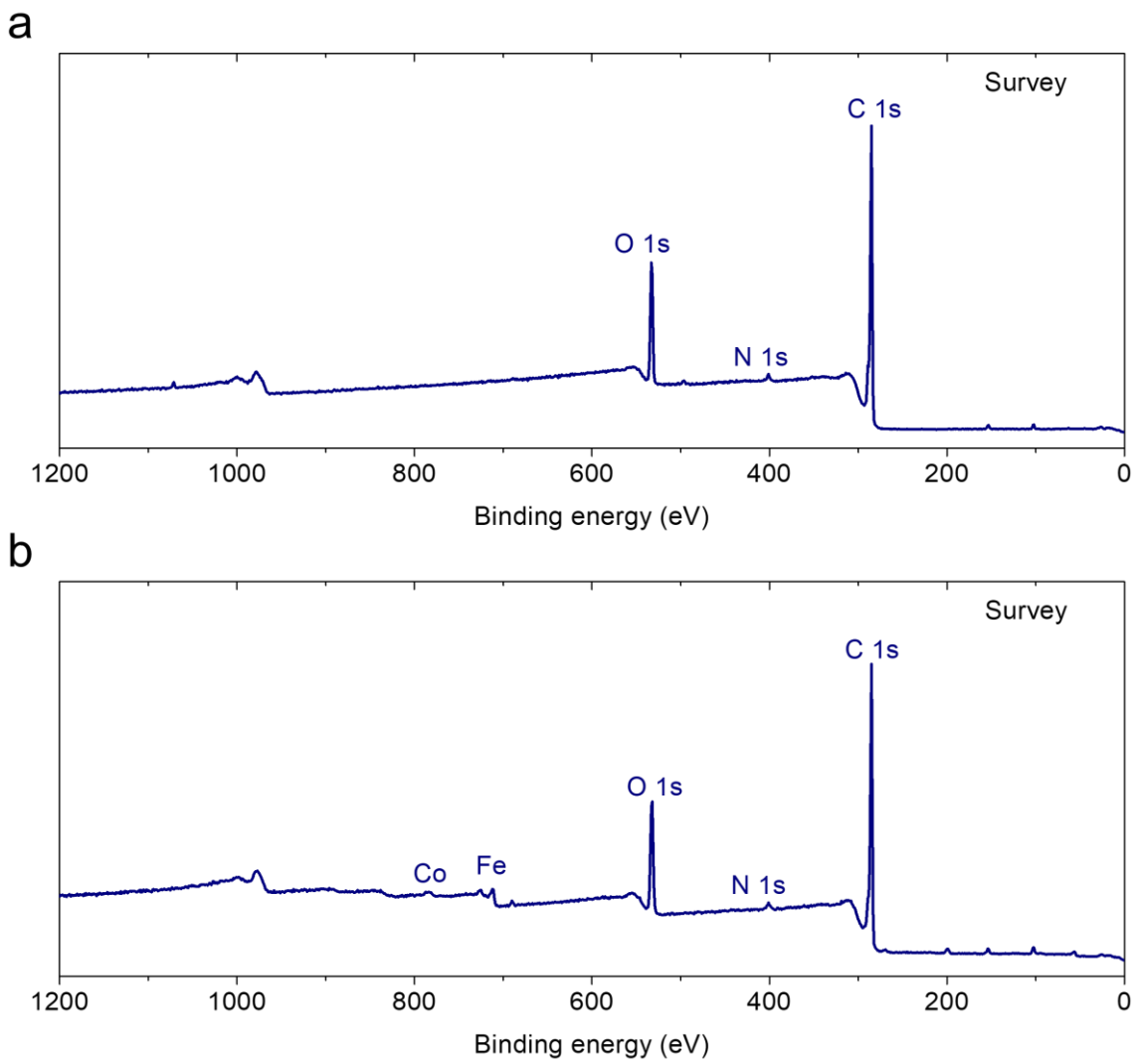

Figure S4. XPS survey spectra of (a) PAN-derived carbon nanofibers and (b) MDPCFs.

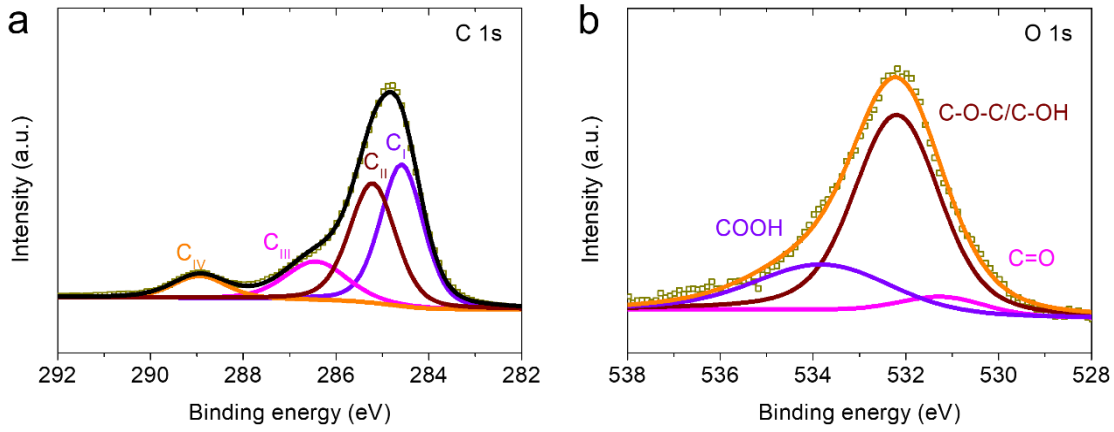

Figure S5. XPS spectra of MDPCFs in (a) C 1s region and (b) O 1s region.

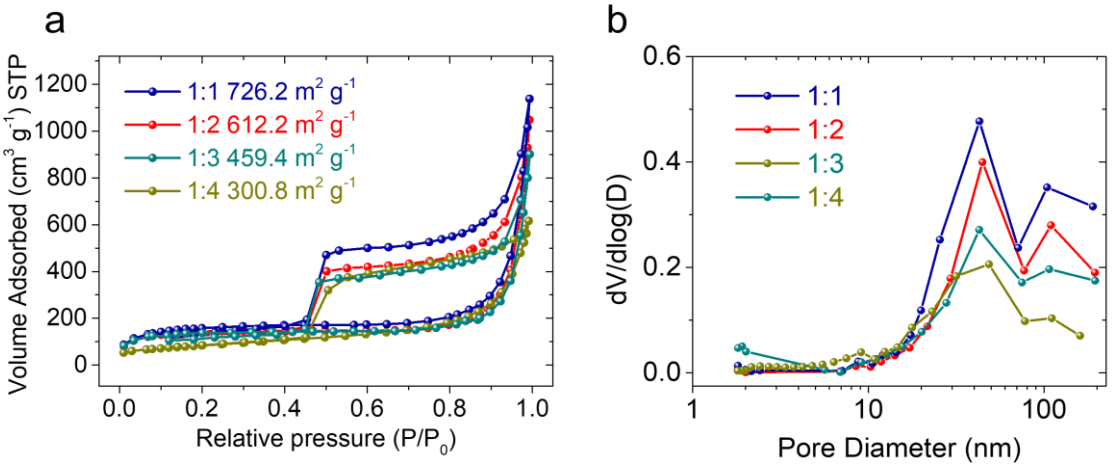

Figure S6. (a) N_2 adsorption/desorption isotherms of MDPCF series samples synthesized using precursors containing different CoFe-glycerate to PAN mass ratios; (b) BJH pore diameter distribution of those samples.

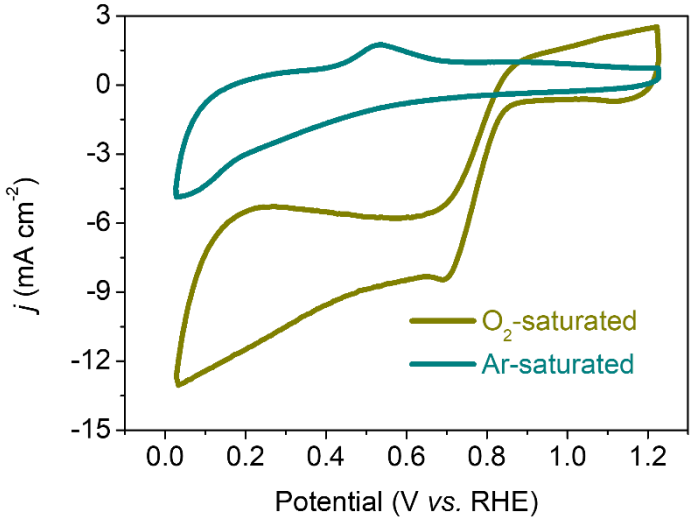

Figure S7. Cyclic voltammograms of MDPCFs recorded at 20 mV s^{-1} in Ar- and O_2-saturated 0.1 M KOH solution.

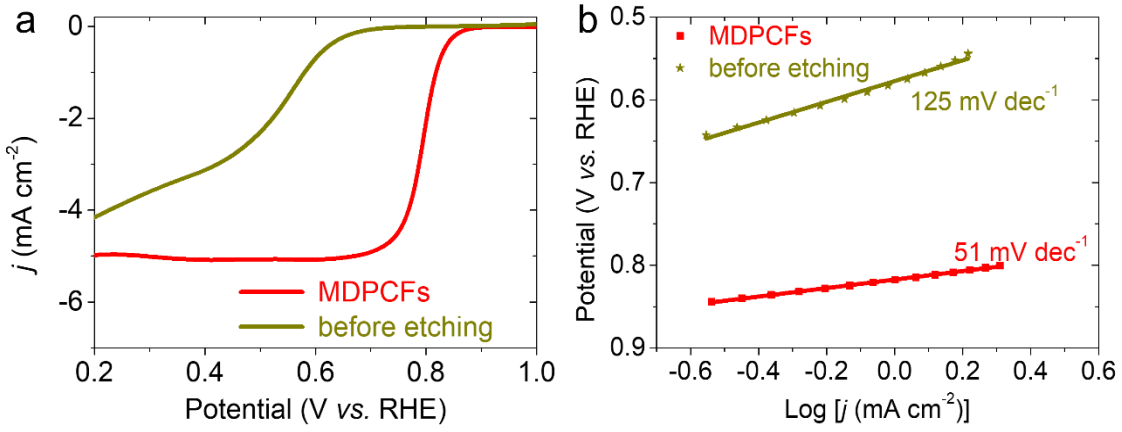

Figure S8. (a) ORR polarization curves of MDPCFs, and the sample before etching in 0.1 M KOH solution at a scan rate of 5 mV s^{-1} and (b) their corresponding Tafel slopes.

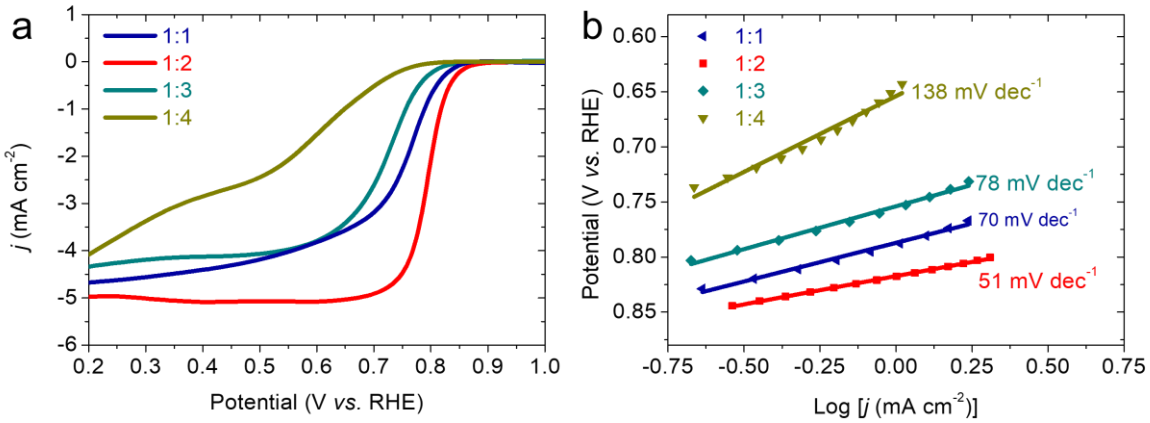

Figure S9. (a) ORR polarization curves of MDPCFs synthesized using precursors containing different CoFe-glycerate to PAN mass ratios and (b) their corresponding Tafel slopes.

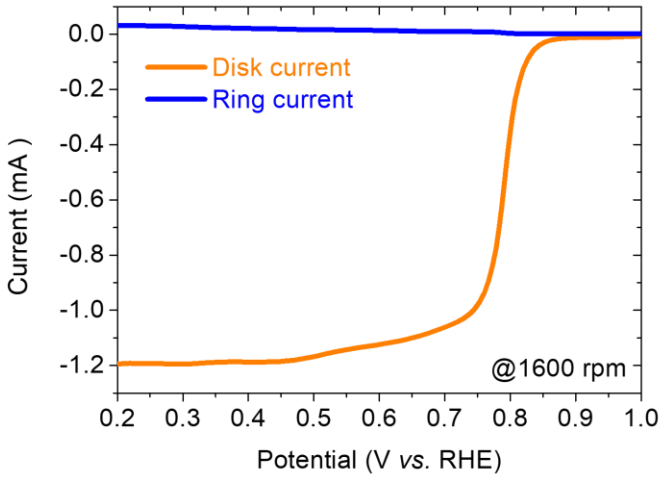

Figure S10. RRDE ORR polarization profiles of MDPCFs at 1600 rpm in 0.1 M KOH solution.

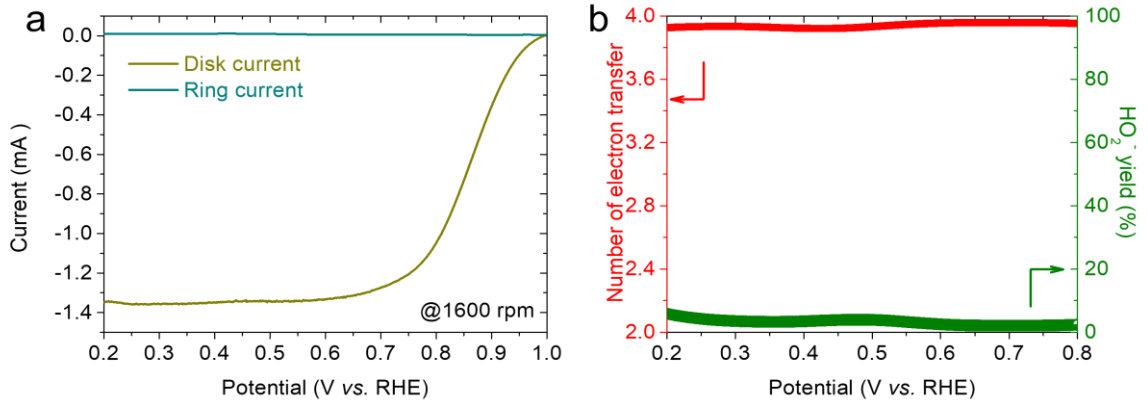

Figure S11. (a) RRDE ORR polarization profiles of Pt/C at 1600 rpm in 0.1 M KOH solution. (b) RRDE-calculated electron transfer numbers and H_2O_2 yields during ORR on Pt/C.

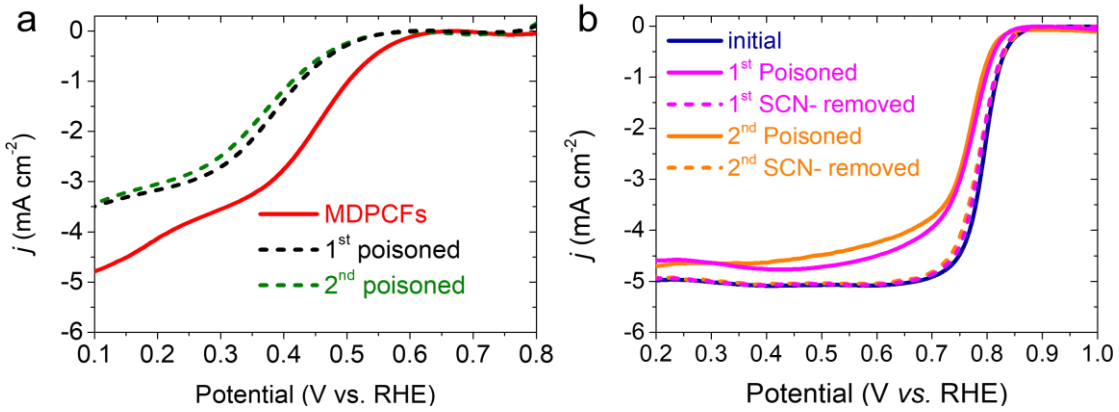

Figure S12. The second poisoning test. (a) ORR curves of MDPCFs in O_2-saturated 0.1 M $HClO_4$ solution before and after the introduction of 5 mM SCN^-. (f) ORR polarization curves of MDPCFs recorded in O_2-saturated 0.1 M KOH solution with or without pre-poisoned by 5 mM SCN^-, and one collected after SCN^- removal.

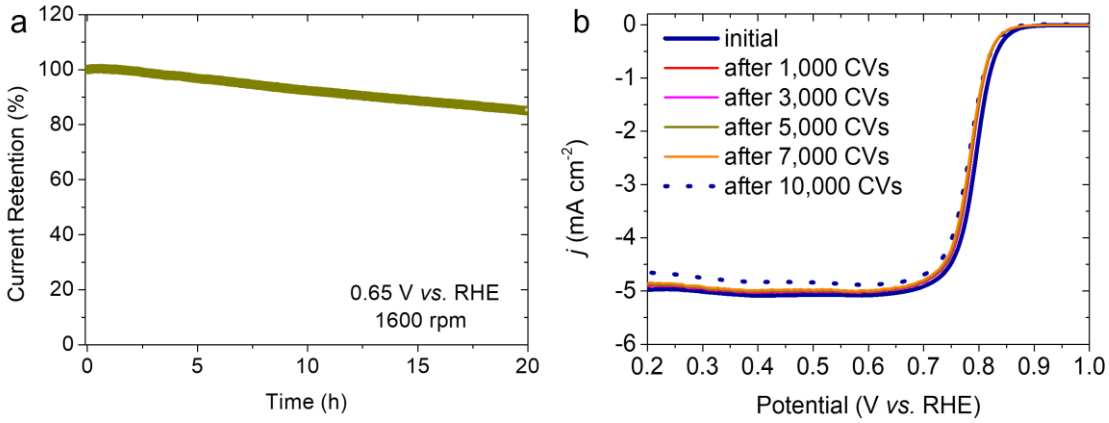

Figure S13. (a) Chronoamperometry measurement of MDPCFs at the potential of 0.65 V *vs.* RHE. (b) Accelerated durability test by cyclic voltammetry at 50 mV s^{-1}. All experiments were conducted in O_2-saturated 0.1 M KOH.

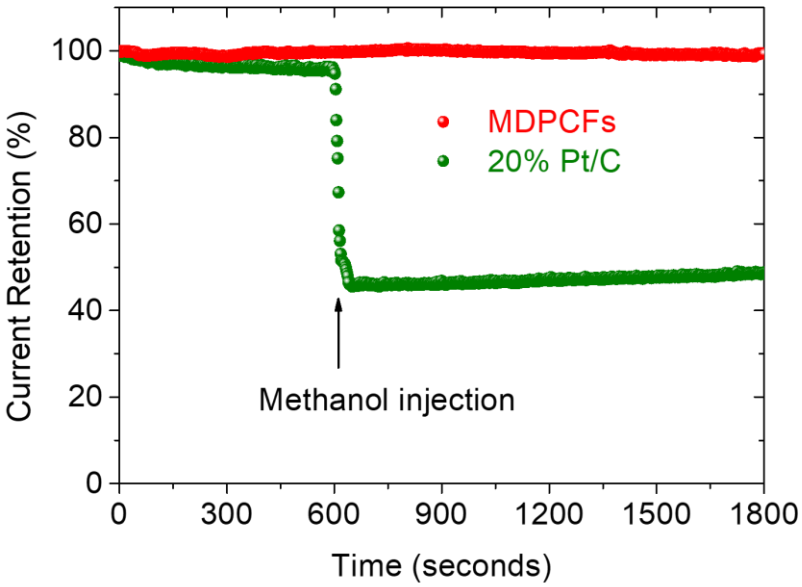

Figure S14. Chronoamperometry responses of MDPCFs and 20 wt.% Pt/C before and after methanol injection.

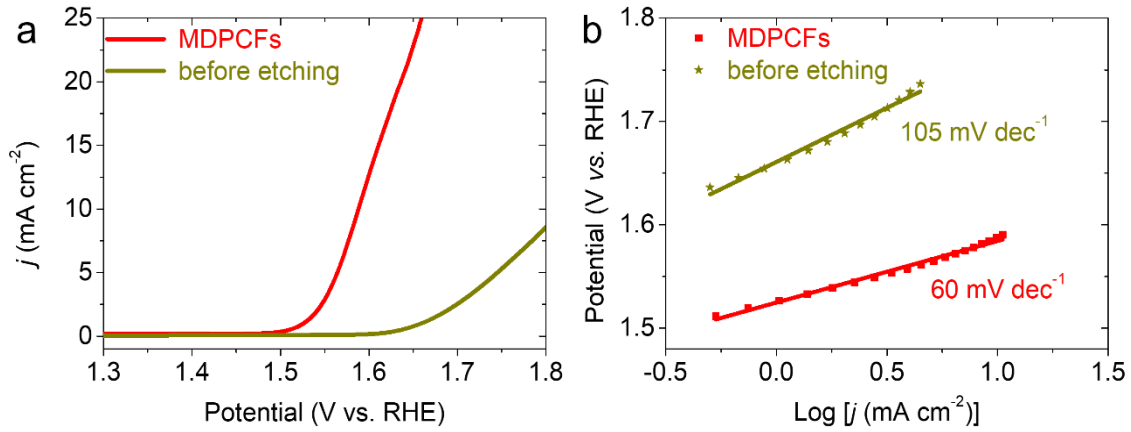

Figure S15. (a) OER polarization curves of MDPCFs, and the sample before etching in 0.1 M KOH solution at a scan rate of 5 mV s^{-1} and (b) their corresponding Tafel slopes.

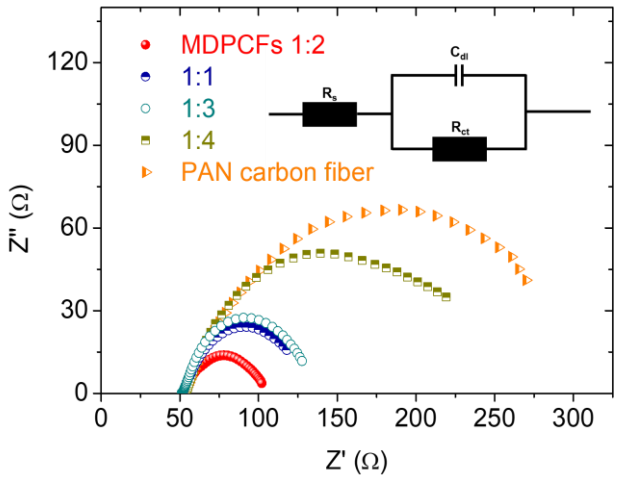

Figure S16. EIS spectra measured at 400 mV OER overpotential of PAN-derived carbon fibers and MDPCFs synthesized using fiber precursors at different CoFe-glycerate to PAN mass ratios.

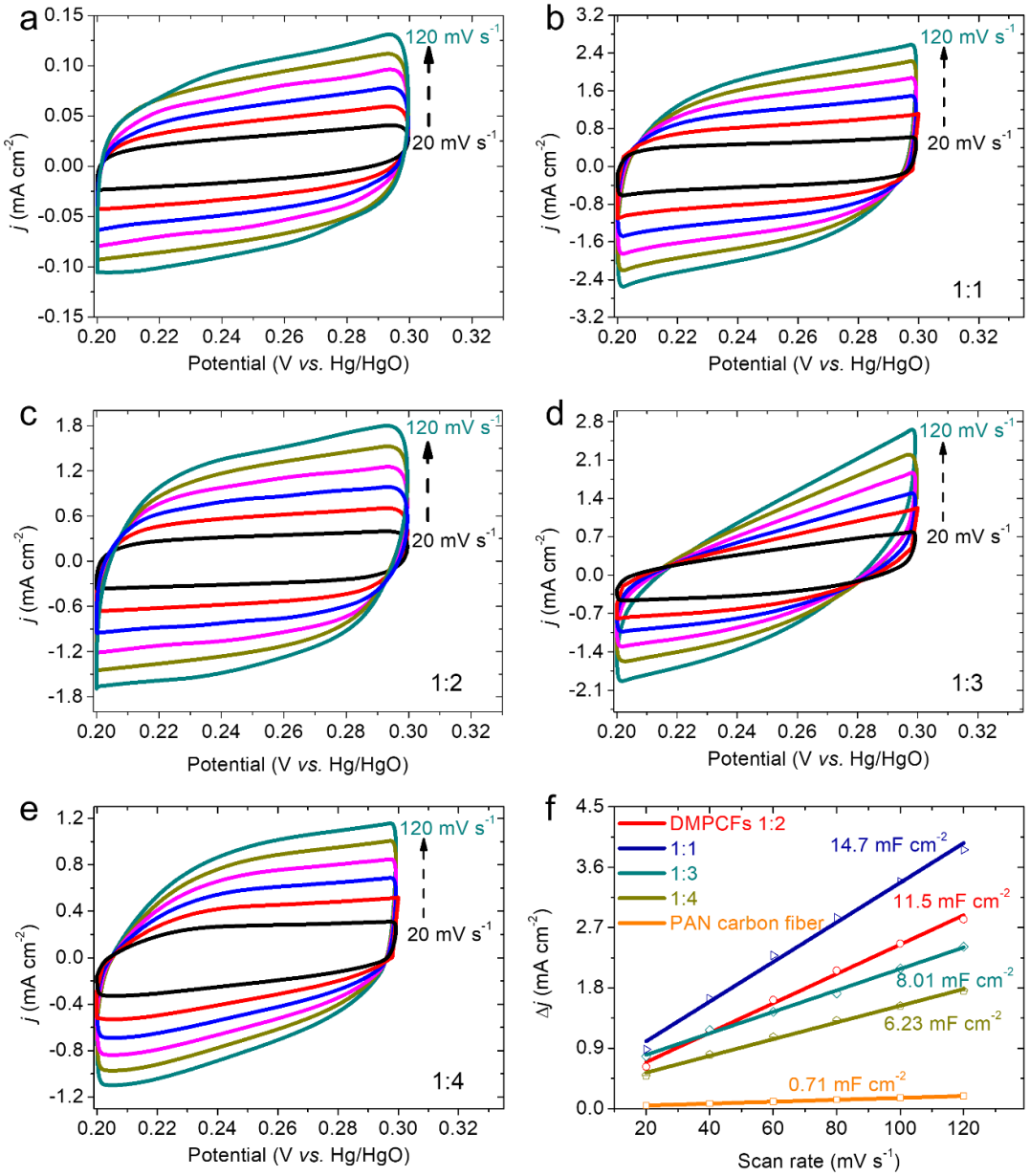

Figure S17. Cyclic voltammograms of (a) PAN-derived carbon nanofibers and (b-e) MDPCFs synthesized using precursors with different CoFe-glycerate to PAN mass ratios (b) 1:1, (c) 1:2, (d) 1:3, (e) 1:4. All CV curves were measured in a potential window of 0.2-0.3 V (vs. Hg/HgO) at various scan rates of 20, 40, 60, 80, 100, and 120 mV s^{-1} in 0.1 M KOH solution. (f) Their corresponding capacitive current (j_{anodic}-$j_{cathodic}$) at 0.25 V (vs. Hg/HgO) as a function of CV scan rates.

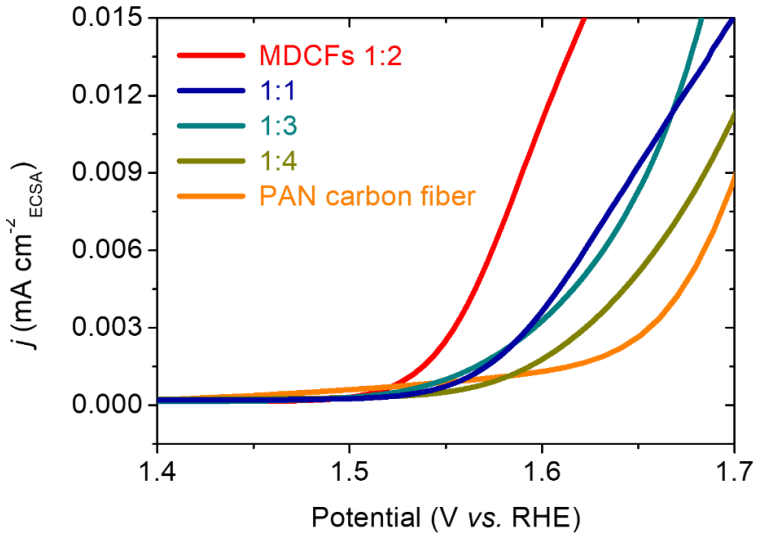

Figure S18. OER polarization curves of PAN-derived carbon nanofibers and MDPCFs synthesized using precursors with different CoFe-glycerate to PAN mass ratios after electrochemically active surface area (ECSA) normalization

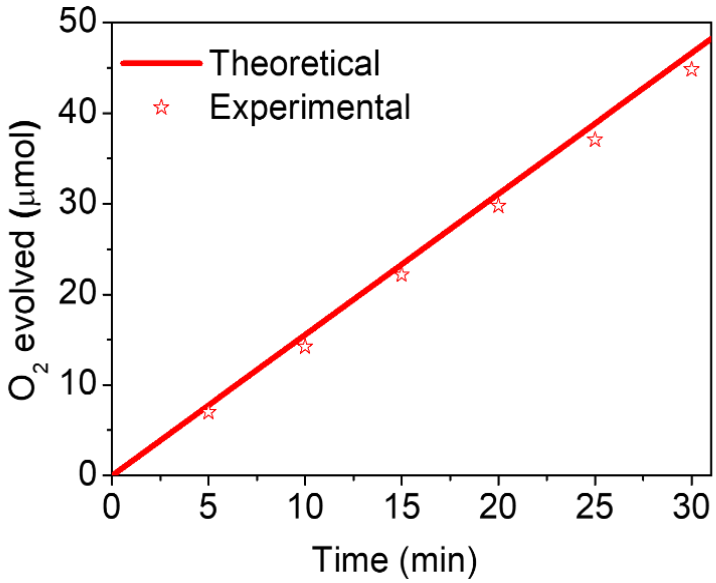

Figure S19. Faradaic efficiency of O_2 generation over MDPCFs under the current of 2 mA for 60 minutes.

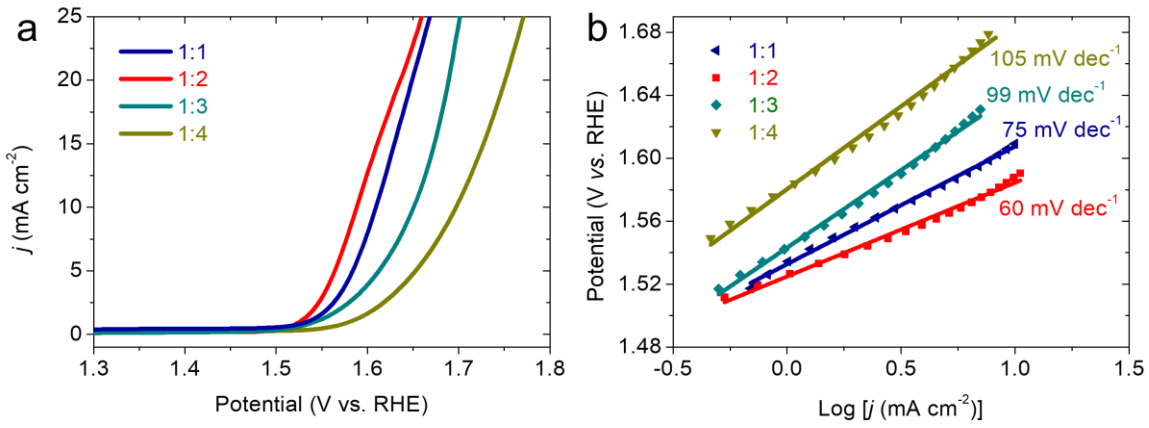

Figure S20. (a) OER polarization curves of MDPCFs synthesized using precursors with different CoFe-glycerate to PAN mass ratios and (b) their corresponding Tafel slopes.

Figure S21. A photo of the A-PAA hydrogel used in this study.

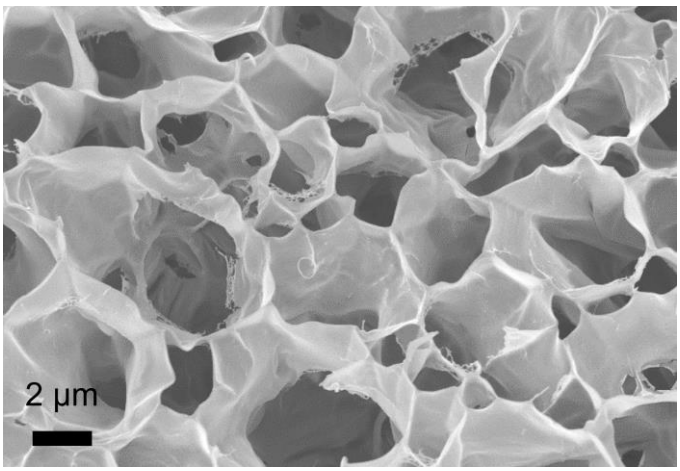

Figure S22. An SEM image of freeze-dried A-PAA hydrogel.

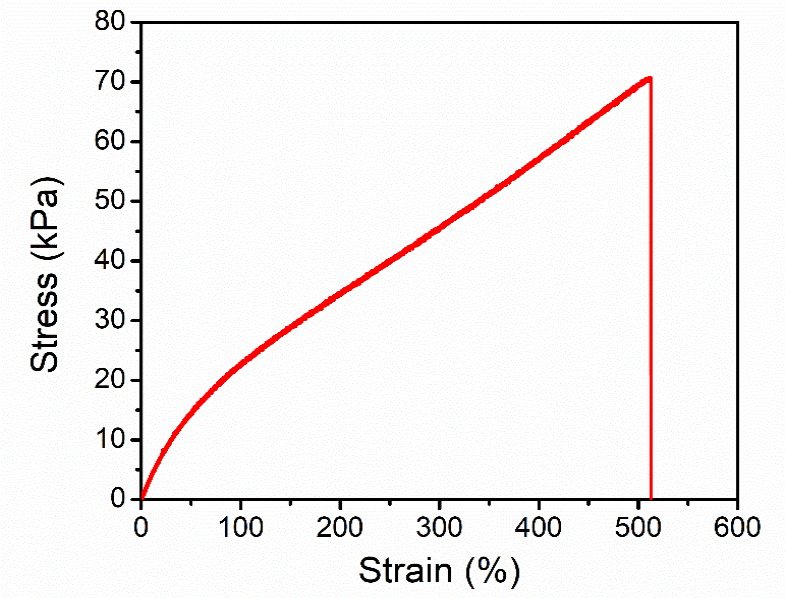

Figure S23. Tensile strain-stress curve of KOH-filled A-PAA hydrogel. The water content of the hydrogel is around 65 wt%.

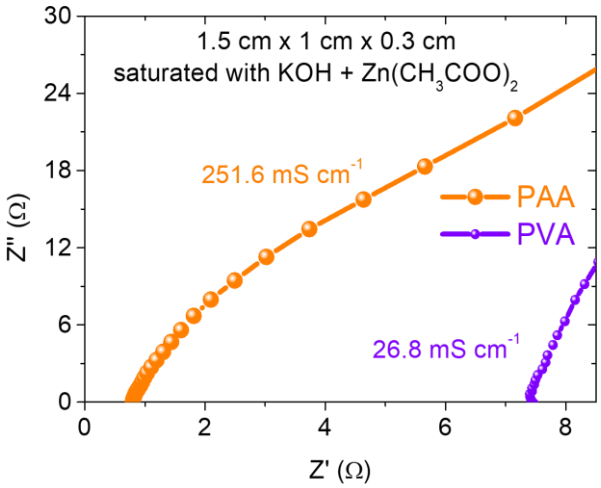

Figure S24. AC impedance spectrum of the A-PAA hydrogel and PVA (1.5 cm (length) x 1.0 cm (width) x 0.3 cm (thickness) in size) saturated with 6 M KOH + 0.2 M $Zn(CH_3COO)_2$.

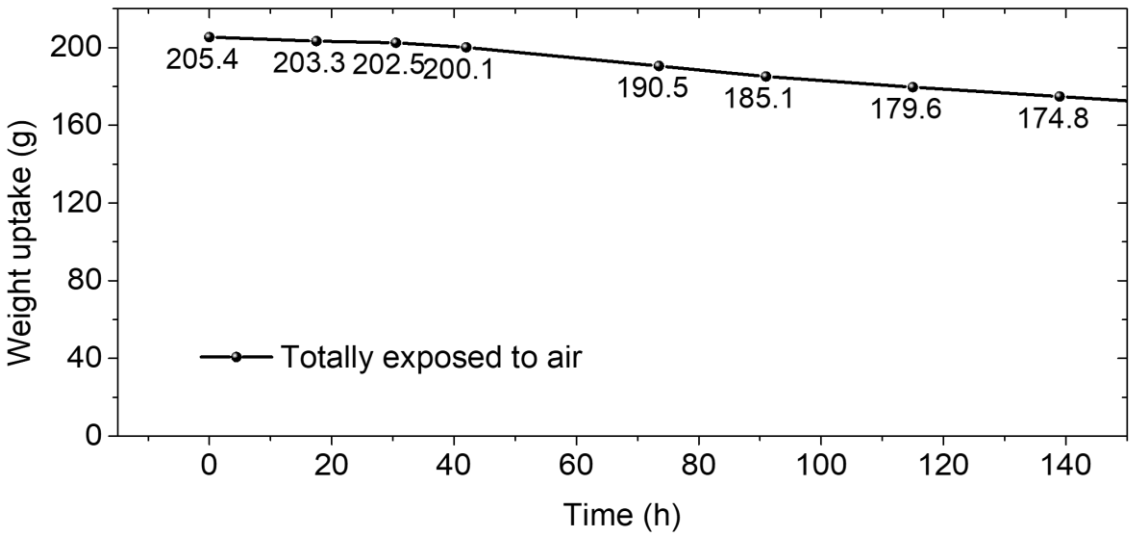

Figure S25. Water retention capability of the A-PAA hydrogel used in this study.

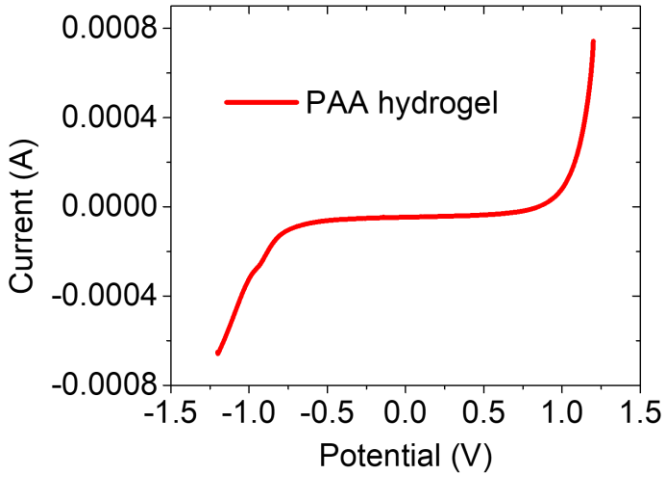

Figure S26. Electrochemical stability windows of A-PAA solid-state electrolyte.

Table S1. XPS quantitative analysis of MDPCFs (1:2) electrocatalyst

Element	Atomic %
C	79.27
N	3.27
O	14.81
Fe	1.39
Co	1.26

Table S2. XPS quantitative analysis of nitrogen species of MDPCFs (1:2) electrocatalyst

	Binding Energy (eV)	Atomic %
N atoms in pyridinic rings	398.17	18.85
Fe(Co)-N_x	399.36	8.38
pyrrolic N	400.28	2.80
graphitic N	401.07	41.33
oxidized N	402.69	28.65

Table S3. Comparison of the catalytic activity of MDPCFs with other bifunctional O_2 electrocatalysts reported in recent publications.

Electrocatalyst	**Mass loading (mg cm^{-2})**	**$E_{1/2}$ (V *vs.* RHE)**	**E_{10} (V *vs.* RHE)**	**ΔE (V)**	**Ref.**
MDPCFs	**0.2**	**0.8**	**1.59**	**0.79**	**This work**
N and Ni codoped np-graphene	0.4	0.845	1.5	0.655	Adv. Mater. **2019**, 1900843
Co SA on N-doped carbon flake arrays grown on carbon nanofibers	0.4	0.88	1.63	0.75	Adv. Mater. **2019**, 31, 1808267
FeN_x/porous N-doped carbon	0.14	0.86	1.62	0.76	ACS Nano, **2018**, 12, 1949
FeNC-S-Fe_xC/Fe	0.1	0.821	1.501	0.68	Adv. Mater., **2018**, 30, 1804504
Activated commercial carbon cloth	-	0.78	1.59	0.81	Adv. Energy Mater. **2018**, 1802936.

NS-carbon cloth	-	0.72	1.59	0.87	Adv. Sci. **2018**, 5, 1800760
Co SA in porous N-doped carbon	1.35	0.86	1.59	0.73	ACS Catal. **2018**, 8, 8961
Co nanoparticles encapsulated into N-doped CNTs	0.81	0.9	1.64	0.74	Adv. Funct. Mater. **2018**, 28, 1705048.
Silk-derived and nitrogen-doped nanocarbon	-	0.764	1.96	1.196	Chem. Mater. **2019**, 31, 1023
Co-CoO/N-rGO	0.21	0.78	1.62	0.84	Adv. Funct. Mater. **2015**, 25, 5799
N/Co-doped PCP//NRGO	0.71	0.86	1.66	0.8	Adv. Funct. Mater. **2015**, 25, 872
Co@Co_3O_4/NC	0.21	0.8	1.65	0.85	Angew. Chem. Int. Ed. **2016**, 55, 4087
Co_3O_4/NPGC	0.2	0.84	1.68	0.84	Angew. Chem. Int. Ed. **2016**, 55, 4977
NiCo/PFC aerogels	0.13	0.77	1.63	0.86	Nano Lett. **2016**, 16, 6516
Co/CoO_x-perovskite nanofibers	0.5	0.76	1.64	0.88	Nano Energy **2017**, 32, 247
Co-N_x-C-graphene	0.25	0.78	*ca.*1.73	0.95	Adv. Mater. **2017**, 29, 1703185
$CoO_{0.87}S_{0.13}$/GN	0.36	0.83	1.59	0.76	Adv. Mater. **2017**, 29, 1702526
FeCo-N-doped CNT	0.2	0.92	1.73	0.81	Adv. Energy Mater. **2017**, 7, 1602420
Co_3O_4/N-doped CNT	3	0.81	1.7	0.89	Small, **2017**, 13, 1700518
Co-N,B-carbon sheet	-	0.84	1.67	0.83	ACS Nano **2018**, 12, 1894

Table S4. Performance comparison of recently reported aqueous rechargeable ZABs

Catalyst	Mass loading (mg cm^{-2})	OCV (V)	P (mW cm^{-2})	Round-trip efficiency	Stability	Ref.
MDPCFs	**1**	**1.48**		**64% @ 10 mA cm^{-2}**	**2000 cycles for >330 h @ 10 mA cm^{-2}**	**This work**
FeCo/FeCoNi@NCNTs-HF	2	1.481	156.22	0.76 V gap	360 cycles for 240 h @ 5 mA cm^{-2}	Appl. Catal. B **2019**, 254, 26
Co/CoNx nanoparticles in nitrogen-doped carbon	1.2	-	-	-	1200 cycles for 400 h @ 10 mA cm^{-2}	Energy Storage Mater. **2019**, 16, 243
single-atom Co–Nx–C	0.1	-	78		164 cycles for 55 h @ 5 mA cm^{-2}	Adv. Mater. **2019**, 31, 1900592
Co3O4 nanowire-assembled clusters on nickel foam	3.9	-	35.7	-	1000 cycles for 330 h @ 10 mA cm^{-2}	Appl. Catal. B **2019**, 241, 104
N, P-codoped porous carbon spheres	-	-	79	-	-	Nano Energy **2019**, 60, 536
Co Nanoparticles Confined in 3D N-Doped Porous Carbon	2	1.44	170	62.5%	500 cycles for 166 h @ 10 mA cm^{-2}	Small **2018**, 14, 1703739
FeNx-PNC	0.86	1.55	278	0.78 V gap	300 cycles @ 10 mA cm^{-2}	ACS Nano **2018**, 12, 1949
Co and Co_3O_4 nanoparticles stitched in porous graphitized shells	0.9	1.45	118.27	0.91 V gap	800 hours @ 10 mA cm^{-2}	Adv. Energy Mater. **2018**, 8 1702900

C-MOF-C2-900	0.5	1.46	105	-	360 cycles for 120 h @ 2 mA cm^{-2}	Adv. Mater. **2018**, 30, 1705431
Core–Shell NiFe@N-Graphite	2	1.482	85	-	120 cycles for 40 h @ 20 mA cm^{-2}	Adv. Funct. Mater. **2018**, 28, 1706928.
Defect-enriched and pyridinic-N graphene	Self-supported	1.43	135	0.95 V gap	250 cycles @ 5 mA cm^{-2}	Adv. Energy Mater. **2018**, 8, 1703539.
FeNi alloy and N-codoped porous carbon	-	-	80.8	0.825 V gap	34.5 cycles for 23 h @ 8 mA cm^{-2}	Energy Storage Mater. **2018**, 12, 277
MO-Co@N-doped carbon (NC, M = Zn or Co)	1.2	1.42	152	63%	385 cycles for 64 h @ 10 mA cm^{-2}	Adv. Funct. Mater. **2017**, 27, 1700795.
$NiCo_2S_4$/N-CNT	1	1.49	147	67.2%	150 cycles @ 10 mA cm^{-2}	Nano Energy **2017**, 31, 541
Ni_3FeN	-	1.547	-	0.7 V gap	309 cycles for 103 h @ 10 mA cm^{-2}	Nano Energy **2017**, 39, 77
$CuCo_2O_4$@C nanotubes	1	1.41	-	0.79 V gap	160 cycles for 80 h @ 2 mA cm^{-2}	Nano Lett. **2017**, 17, 7989
ZIF-8@ZIF-67 core-shell	1	1.3	-	-	140 cycles for 140 h @ 5 mA cm^{-2}	Nano Energy **2016**, 30, 368
Mn/Fe-HIB-MOF	0.5	1.48	195	62.33%	6000 cycles for >1000 h @ 10 mA cm^{-2}	Energy Environ. Sci., **2019**, 12, 727-738
Sulfur-modulated holey C_2N aerogels	0.5	1.49	209	62.1%	375 cycles for 750 h @ 10 mA cm^{-2}	ACS Nano **2018**, 12, 1, 596-608

P, S codoped C_3N_4 sponges sandwiched with C nanocrystals	0.5	1.51	198	0.8 V gap	500 cycles for 100 h @ 25 mA cm^{-2}	ACS Nano **2017**, 11, 1, 347-357

Table S5. Performance comparison of recently reported flexible rechargeable ZABs.

Catalyst	**Mass loading (mg cm^{-2})**	**Electrolyte**	**Cell structure**	**OCV (V)**	**P (mW cm^{-2})**	**Round-trip efficiency**	**Stability**	**Ref.**
MDPCFs	**1**	**Polyacrylate-KOH**	**Sandwich**	**1.42**	**188.6**	**64% @ 2 mA cm^{-2}**	**500 cycles for >83 h @ 2 mA cm^{-2}**	**This work**
N and Ni codoped np-graphene	0.4	PVA-KOH	Sandwich	1.35	83.8	-	258 cycles for 43 h @ 2 mA cm^{-2}	Adv. Mater. **2019**, 900843
Co SA on N-doped carbon flake arrays on carbon fibers	1.2	PVA-KOH	Sandwich	1.41	-	67%	90 cycles for 15 h @ 6.25 mA cm^{-2}	Adv. Mater. **2019**, 31, 1808267
FeN_x/porous N-doped carbon	0.14	PVA-KOH	Sandwich	1.436	118	60.8%	220 cycles for 40 h @ 5 mA cm^{-2}	ACS Nano, **2018**, 12, 1949
CNT+porphyrin COF	1.5	PVA-KOH	Sandwich	1.39	22.3	61.6% @ 1.0 mA cm^{-2}	-	Energy Environ. Sci. **2018**, 11, 1723
FeNC-S-Fe_xC/Fe	0.5	PVA-KOH	Sandwich	1.41	149.4	55.6	380 cycles for 48 h @ 2 mA cm^{-2}	Adv. Mater., **2018**, 30, 1804504
Activated commercial carbon cloth	-	PVA-KOH	Sandwich	1.37	52.3	51.7% @ 1 mA cm^{-2}	1000 min	Adv. Energy Mater. **2018**, 1802936.
NS-doped carbon cloth	-	PVA-KOH	Sandwich	1.247	47	<60%	20 cycles at 5 mA cm^{-2}	Adv. Sci. **2018**, 5, 1800760
Co SA in porous N-doped carbon	1.35	PAA-KOH	Sandwich	1.41	20.9	-	125 cycles for 2500 min	ACS Catal. **2018**, 8, 8961
Co nanoparticle encapsulated into N-doped CNTs	1	PVA/PEO-KOH	Sandwich	1.345	101	61.1	130 cycles for 15 h @ 2 mA cm^{-2}	Adv. Funct. Mater. **2018**, 28, 1705048.
Silk-derived and nitrogen-doped nanocarbon	2	PVA-KOH	Sandwich	-	32.3	-	130 cycles @ 1 mA cm^{-2}	Chem. Mater. **2019**, 31, 1023

RuO_2-CNT sheet	-	PVA-PEO-KOH	Fiber	1.29	5.7 Wh L^{-1}	53% @ 1 A g^{-1}	30 cycles for 30 h @ 1 A g^{-1}	Angew. Chem. Int. Ed. **2015**, 54, 15390
Co_4N/Co-N-C	-	PVA-KOH	Cable	1.35	-	53% @ 1 mA cm^{-2}	36 cycles for 12 h @ 1 mA cm^{-2}	J. Am. Chem. Soc. **2016**, 138, 10226
N-doped porous carbon fiber	2	PVA-KOH	Sandwich	1.26	-	56% @ 2 mA cm^{-2}	18 cycles for 6 h @ 2 mA cm^{-2}	Adv. Mater. **2016**, 28, 3000
CoO_x on carbon paper	1	Laminate nanocellulose/GO	Sandwich	1.4	44.1	55% @ 1 mA cm^{-2}	30 cycles for 10 h @ 1 mA cm^{-2}	Adv. Energy Mater. **2016**, 6, 1600476
Co-N_x-C-graphene	1.5	PVA-KOH	Sandwich	1.44	30	63% @ 1 mA cm^{-2}	18 cycles for 1 h @ 1 mA cm^{-2}	Adv. Mater. **2017**, 29, 1703185
FeCo-N-doped CNT	-	PVA-KOH	Sandwich	1.25	97.8	48% @ 100 mA cm^{-2}	72 cycles for 12 h @ 100 mA cm^{-2}	Adv. Energy Mater. **2017**, 7, 1602420
$CuCo_2O_4$/N-doped CNT	-	PVA-KOH	Sandwich	1.24	1.86 W g^{-1}	-	27 cycles for 9 h @ 0.5 A g^{-1}	Adv. Funct. Mater. **2017**, 27, 1701833
Co_3O_4 on carbon cloth	-	PVA-KOH	Sandwich	1.32	-	53% @ 2 mA cm^{-2}	30 cycles for 10 h @ 2 mA cm^{-2}	Adv. Energy Mater. **2017**, 7， 1700779
Co_3O_4/N-doped CNT	3	PVA-KOH	Sandwich	1.3	-	50% @ 2 mA cm^{-2}	20 cycles for 20 h @ 2 mA cm^{-2}	Small, **2017**, 13, 1700518
NiO/CoN nanowires on carbon cloth	-	PVA-KOH	Cable	1.34	-	-	50 cycles for 500 min @ 3 mA cm^{-2}	ACS Nano **2017**, 11, 2275
Co-N,B-carbon sheets	0.5	PVA-KOH	Sandwich	1.35	-	50% @ 2 mA cm^{-2}	-	ACS Nano **2018**, 12, 1894
Mn/Fe-HIB-MOF	0.5	Functionalized Biocellulose membrane	Sandwich		193	65.24%	3600 cycles for 600 h @ 10 mA cm^{-2}	Energy Environ. Sci., **2019**, 12, 727-738
Sulfur-modulated holey C_2N aerogels	0.5	Functionalized Biocellulose membrane	Sandwich	1.47	187	-	230 cycles for 460 h @ 25 mA cm^{-2}	ACS Nano **2018**, 12, 1, 596-608

References cited in the ESI:

ESI-1. D. C. Grahame. Chem. Rev. **1947**, 41, 441.
ESI-2. J. D. Benck, Z. Chen, L. Y. Kuritzky, A. J. Forman, T. F. Jaramillo. ACS Catal. **2012**, 2, 1916.